Batteries & Supercaps

Review
doi.org/10.1002/batt.202400437

Chemistry Europe
European Chemical Societies Publishing

www.batteries-supercaps.org

The Role and Substitution of Cobalt in the Cobalt-Lean/Free Nickel-Based Layered Transition Metal Oxides for Lithium Ion Batteries

Taifan Yang,[a] Zhenxin Huang,[a] Chengyong Shu,*[a] Xiaowei Wang,[c] Zexun Tang,*[d] Wei Tang,*[a, b] Kai Zhu,[e] and Yuping Wu[f]

The Nickel-based layered transition metal oxide cathode represented by NCM ($LiNi_xCo_yMn_zO_2$, $x+y+z=1$) and NCA ($LiNi_xCo_yAl_zO_2$, $x+y+z=1$) is widely used in the electric vehicle market due to its specific capacity and high working potential, in which Cobalt (Co) plays a huge role in improving the structural stability during the cycle. However, the limited supply of Co, due to its scarcity and the influence of geopolitics, poses a significant constraint on the further advancement of the Nickel-based layered transition metal oxide cathode in the field of energy storage. In this paper, the mechanism of Co in the Nickel-based layered transition metal oxides is reviewed, including its critical role for structural stability such as the inhibition of cationic mixing and the release of lattice oxygen et al. Subsequently, it outlines various strategies to enhance the performance of Co-lean/free materials, such as ion doping, including single-ion doping and multi-ion co-doping, and various surface coating strategies, so as to eliminate the adverse effects of Co loss on materials. Ultimately, this paper offers a glimpse into the promising future of Cobalt-free strategies for high performance of Nickel-based layered transition metal oxides.

1. Introduction

With the energy crisis and environmental pollution caused by non-renewable resources such as coal and oil becoming increasingly serious, the exploration and utilization of new renewable energy sources have become a pivotal research focus for researchers. To integrate new renewable energy sources into the grid, a large number of energy storage devices are required. Lithium-ion batteries (LIBs) have remained at the forefront of distributed energy storage, electric vehicles and mobile electronic devices due to their high capacity, excellent energy density and security.[1–3] As demand grows, there's an increasing emphasis on improving the energy density and reducing the production cost of LIBs. LIBs are composed of cathode, anode, electrolyte, separator and current collector. Notably, the cathode material accounts for approximately 41% of the battery's total weight and a significant portion of its manufacturing cost.[4] Therefore, researchers are continually striving to pursue cathode materials with high capacity, long-term cyclability as well as lower cost.[5,6]

The Nickel-based Layered transition metal oxide materials such as $LiNi_xCo_yMn_zO_2$ (NCM, $x+y+z=1$) and $LiNi_xCo_yAl_zO_2$ (NCA, $x+y+z=1$) have garnered significant attention and are widely utilized as cathode materials for lithium-ion batteries.[7,8] Evolving from lithium cobaltate material, NCM cathode material was first proposed in 1980,[9] in which the increase of Ni content is believed to improve the charge and discharge capacity of the material while Co plays a positive role in reducing the mixing of cations in the material.[10,11] Moreover, Mn is deemed to play a crucial role in improving the structural stability and integrity of the material.[12–14]

However, owing to its low abundance and geopolitical concerns, Co is perceived as the most significant risk factor in the electric vehicle supply chain in the short and medium term. Given the concerns over battery cost and supply risks, researchers and commercial companies have reached a certain consensus to minimize or eliminate the existence of Co without sacrificing performance.[15,16]

The reduction of cationic mixing is believed to improve the structural stability and thermal stability of Nickel-based Layered transition metal oxide materials.[17–21] However, the mechanism of how the presence of Cobalt reduces the mixing of cations is still unclear. Some researchers believe Cobalt inhibits Li/Ni mixing by forming a weak super-exchange structure with antiposition Ni^{3+},[22–25] while others hold the view that Co^{3+}

[a] T. Yang, Z. Huang, C. Shu, W. Tang
School of Chemical Engineering and Technology, Xi'an Jiaotong University, Xi'an 710049, China
E-mail: kowscy-n@mail.xjtu.edu.cn
tangw2018@mail.xjtu.edu.cn

[b] W. Tang
Innovation Platform (Center) for Industry-Education Integration of Energy Storage Technology, Xi'an 60439710049, China

[c] X. Wang
Chemical Sciences and Engineering Division, Argonne National Laboratory, 60439 Lemont, IL, USA

[d] Z. Tang
College of Materials and Chemical Engineering, Hunan Institute of Engineering, Xiangtan 411104, China
E-mail: tangzexun@163.com

[e] K. Zhu
Shanghai Institute of Space Power-Sources (SISP), Shanghai Academy of Spaceflight Technology, Shanghai 200233, China

[f] Y. Wu
School of Energy and Environment, Southeast University, Nanjing 210096, China

inhibits the Li/Ni mixing by eliminating the reluctance and lowering the system energy.[26–28] Moreover, some researchers have observed that Co^{3+}impedes the migration of Ni by occupying the cohedral tetrahedral position between the Li octahedral position and transition metal layer octahedral position.[29–31] Due to the complex role of Co in the Nickel-based layered transition metal oxide cathode, direct substitution or elimination of Co with Ni or Mn in the material may cause dramatic degradation of the performance in terms of specific capacity and cyclability. For instance, Zhong et al verified the substitution of manganese for Cobalt in Ni80 ($LiNi_{0.8}Co_xMn_{0.2-x}$) material,[32] and the result was not satisfactory. With the substitution of Mn for Co, the specific capacity of the material has a great loss, and at the same time, the cyclic performance, rate performance and internal resistance value of the material also have a large landslide. This indicates that the strategy of simply replacing Co with Mn is not feasible.

To maintain the performance of Nickel-based layered transition metal oxide materials while eliminating the Co element, it is imperative to devise a stable and high-energy-density Co-free high Ni layered oxide through the precise doping and substitution of various elements in appropriate quantities. Therefore, uncovering the underlying mechanism of the critical role played by Co element in the Nickel-based layered transition metal oxide cathode material is of utmost significance. In this regarding, the mechanism of reducing cationic mixing and improving material stability of Co in the Nickel-based layered transition metal oxide cathode materials is firstly discussed. Additionally, it presents proper Co-free/eliminating strategies in cathode materials, encompassing ion doping and surface coating techniques (Figure 1). Following by the comparison of these strategies, this review tried to outline a perspective guideline for future development of Co-free/lean Nickle-based layered transition metal oxides cathodes.

2. Critical Role of Cobalt in the Nickel-based Layered Transition Metal Oxides

2.1. Inhibit Cationic Mixing

The Nickel-based layered transition metal oxide material is comprised of alternating layers of lithium and transition metal (TM) ions, interspersed with layers of oxygen atoms. During synthetic and electrochemical cycles, a migration occurs, where some transition metal atoms shift to the Li site, while some Li atoms occupy the transition metal site, inducing Li/Ni exchange or Li/Ni mixing between the Li and TM layers.[6,33–37] This Li/Ni mixing significantly impacts the properties of Nickel-based layered transition metal oxide mainly in three principle ways: (i) The inverse Ni^{2+}oxidizes to $Ni^{3+}$with smaller ionic radius during the cycle, leading to the collapse of the Li diffusion channel and a reduction in the Li layer thickness, thereby decreasing the Li ion diffusion coefficient. As studied by KANG et al, a slight reduction of the Li layer space by 0.02 μm, may result in an increase in the activation barrier of 20 to 30 meV.[38,39] (ii) The inverse Ni^{2+} in the Li layer tends to migrate towards the particle surface during cycling, reducing the Ni content within the particle, which subsequently decreases the voltage and capacity of the material.[40,41] (iii) Li/Ni exchange leads to anisotropic stresses in the material, accelerating structural degradation during cycling and diminishing the cycle performance.[42] Although some studies have shown that appropriate cationic mixing can improve the stability of materials to a certain extent, it is indisputable that cationic mixing generally has a profound negative effect on the stability of Nickel-based layered transition metal oxide materials.

In the past, it was commonly held that primary impetus behind Li/Ni mixing stemmed from the comparable ionic radius of Li^{+}0.76 Å and Ni^{2+}0.69 Å, creating a spatial arrangement conducive to the effortless interchange of Li and Ni.[43–46] While

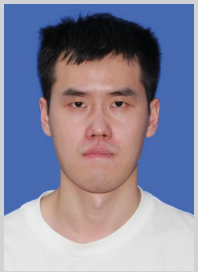

Taifan Yang received his B.E degree (2023) from Xi'an Jiaotong University. Now, he is pursuing themaster's degree at School of Chemical Engineering and Technology, Xi'an Jiaotong University. His research interests focus on the design and synthesis of cathode for sodium ion batteries.

Chengyong Shu serves as an associate professor within the School of Chemical Engineering and Technology at Xi'an Jiaotong University, and is affiliated with the Institute of Materials Chemical Engineering. He obtained his Ph.D. in materials science and engineering from Xi'an Jiaotong University in 2018. Dr. Shu's research portfolio encompasses advanced fuel cell technologies, including hydrogen-oxygen and hydrogen-air systems, as well as medium to high-temperature fuel cells. His expertise extends to the realm of lithium and sodium-ion batteries, with a particular focus on lithium iron phosphate cathodes, layered oxide cathodes, and carbon-based anodes.

Wei Tang is now a professor at School of Chemical Engineering and Technology, Xi'an Jiaotong University. He received his B.S. from Nanjing University of Science and Technology, China, in 2009 and his Ph.D. from the department of chemistry in the National University of Singapore in 2016. He was awarded the NUS Graduate School for Integrative Sciences and Engineering (NGS) scholar ship. Dr. Tang's research focuses on design and fabrication of novel nanomaterials for the applications in new generation energy storage and conversion, such as supercapacitors and Li-/Na-/K-ion batteries.

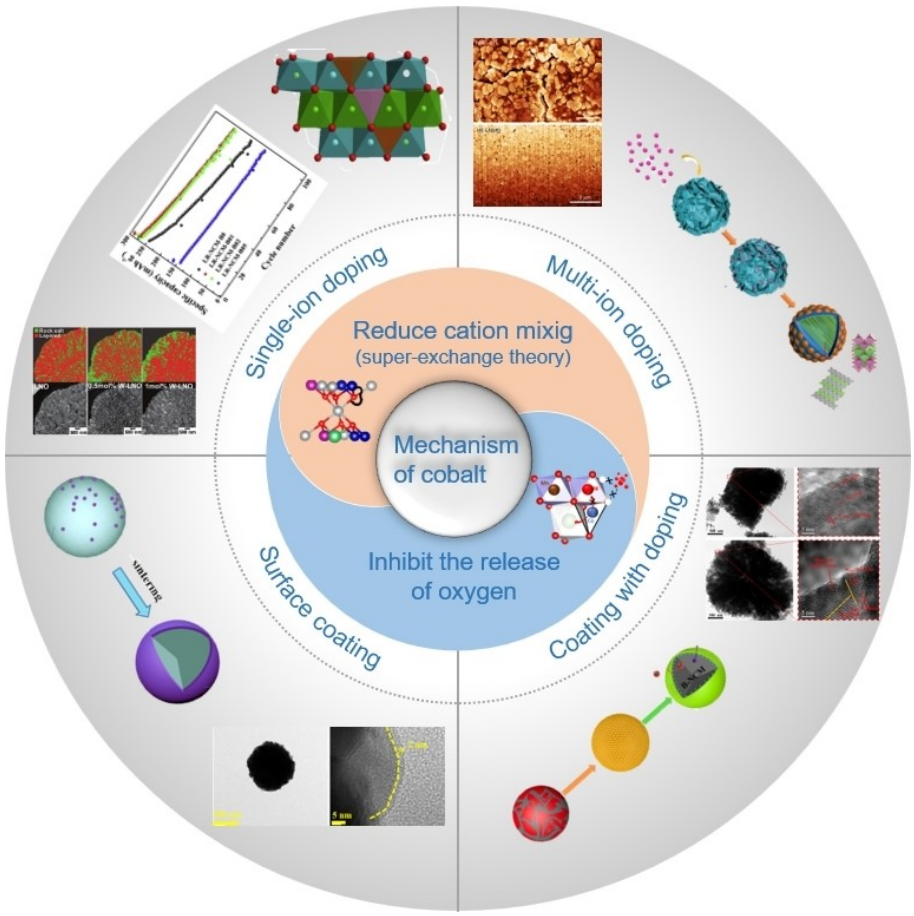

Figure 1. The action mechanism of Cobalt in Nickel-based transition metal layer oxides and the Cobalt-free strategy of cathode materials.

Li/Ni mixing tends to occur in materials with higher Ni^{2+} content according to this theory, it fell short of explaining why Ni/Li exchange occurs even more frequently in Ni-rich NMC materials where most Ni cations are Ni^{3+}. To compensate this theory, at present, many researchers posit that the super-exchange interaction between transition metals holds significant sway in governing cation disorder.[37]

Pursuant to the super-exchange theory, the interchange between magnetic ions in antiferromagnetic substances is facilitated by non-magnetic ions positioned centrally.[47–49] Ni^{2+}/Ni^{3+} forms a 90° intra-layer super-exchange with neighboring TM cations by bridging the O anion in the TM layer, due to the presence of unpaired electrons in d orbitals. When the Li/Ni exchange occurs, the anti-Ni ion at the Li position possesses a magnetic moment that is opposite to the Ni ion at the TM position, thereby forming a σ bond with the p orbital of O through the e_g orbital of the anti-Ni ion. Consequently, a 180° linear super-exchange structure with transition metal ions Ni^{2+}, Ni^{3+}, and Mn^{4+} is readily in the TM layer (Figure 2a, b). However, owing to the robust σ bond, the 180° super-exchange structure formed by the inverse Ni ion with the transition metal ion is inherently more stable than the 90° one created by the Ni ion with the adjacent transition metal ion in the TM layer, yielding a thermodynamic advantage of the Li/Ni exchange.[47,48,50] As a result, a weaker 180° super-exchange interaction between the TM cation and the inverse Ni^{2+} corresponds to a reduced degree of Li/Ni mixing. Different from direct interaction, O ion plays the role of a carrier in the super-exchange interaction.[23] The p orbitals of intervening oxygen participate in the super-exchange interaction via the formation of the σ bond between the d orbital of TM cations and the p orbital of O^{2-}. The transfer of an electron from the pσ-orbital to one of the neighboring TM cations causes an unpaired spin left on O^{2-}, which couples to the spin of the other neighboring TM cation through exchange interaction. So, the strength of super-exchange interactions can be reflected by the spin density of the O ion. Thus 3D spin electron density maps can be used to analyze the strengths of different kinds of 180° super-exchange interactions.[49]

Figure 2e–i portray a 3D spin-electron density map of different types of 180° super-exchange interactions.[23] Due to the two unpaired electrons of Ni^{2+}, it can be seen that among the linear super-exchanges, the spin density of O^{2-} in the linear antiferromagnetic (AF) Ni^{2+}–O^{2-}–Ni^{2+} is the most prominent, signifying the strongest super-exchange interaction. The linear ferromagnetic (FM) Ni^{2+}–O^{2-}–Mn^{4+}(e_g–2p–t_{2g}) and FM Ni^{2+}–O^{2-}–Co^{4+}(e_g–2p–t_{2g}) super-exchanges exhibit weaker interactions, while the linear AF Ni^{2+}–O^{2-}–Ni^{3+}(e_g–2p–e_g) super-exchange falls in the moderate range. Notably, the absence of unpaired electrons in the electronic configuration of Co^{3+} renders the Ni^{2+}–O^{2-}–Co^{3+} super-exchange the weakest, thus

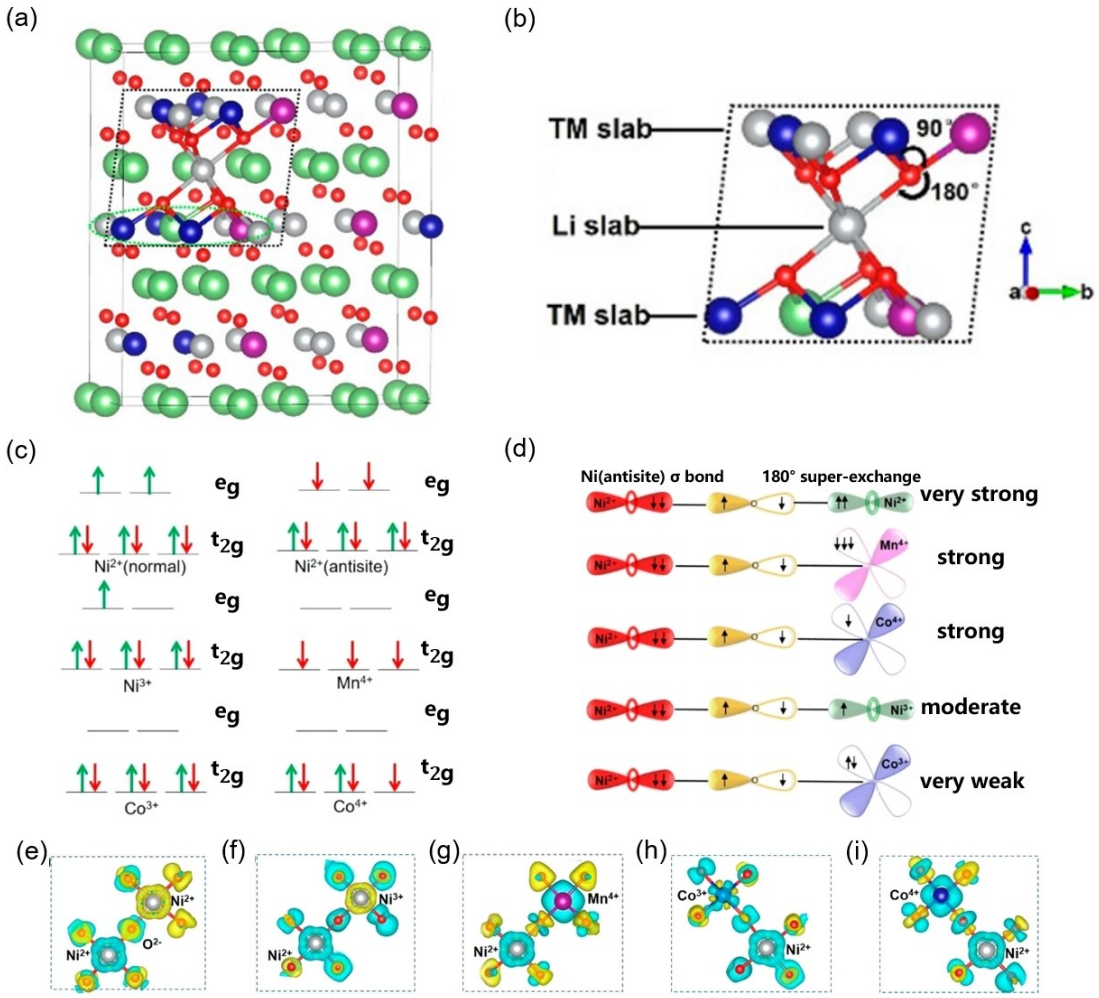

Figure 2. (a) Structure model for the multilattice of $Li(Ni_{0.6}Mn_{0.2}Co_{0.2})O_2$ (622) with one pair of Ni/Li exchange. (b) $(TM)_6$–O_3–Ni–O_3–$Li(TM)_5$ coordination structure unit for the antisite Ni in Li slab. Green: Li; red: O; silver: Ni; purple: Mn; blue: Co. (c) Electronic configurations for TM ion in NMC materials. (d) Schematic for 180° super-exchange interaction. (e-i) 3D spin electron density maps of different kinds of 180° super-exchange interactions. Blue and yellow denote spin up and spin down, respectively. The isovalues for the isosurfaces of the spin densities were 0.05 $eÅ^{-3}$ for all cases.[23] Copyright (2017) American Chemical Society.

explains why the presence of Co inhibits the mixed arrangement of Li/Ni.

In addition, Wang et al investigated the magnetic interaction between transition metal ions and postulated that the cause of Li/Ni mixing cannot only consider the volume factor,[26] and magnetic interaction also plays a key role. As shown in Figure 3, since Ni possesses a relatively strong magnetic moment, the Ni^{2+}cations placed in three triangles inevitably have two opposite magnetic moments, compelling the structure to shift to a higher energy level and more unstable state, thereby inducing a "magnetic frustration".[28,51–53] On the other hand, owing to no magnetic moment of Li ion, the exchange of Li/Ni position can effectively mitigate the magnetic frustration, reducing the system's energy, which serves as the thermodynamic basis of Li/Ni mixed arrangement. Similarly, Co^{3+}also has no magnetic moment, can occupy Ni positions, thereby eliminating the reluctance and reducing the system energy, ultimately inhibiting the Li/Ni mixing.[54,55]

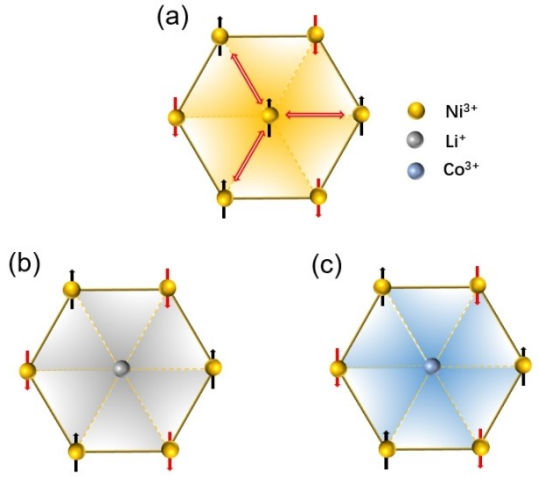

Figure 3. The magnetic interactions of (a) Ni^{3+}, (b) Li^{+}, (c) $Co^{3+}$with the Ni^{3+}nearby.

2.2. Inhibit Lattice Oxygen Release

The poor thermal stability of Ni-rich layered transition metal oxides, particularly under high delithium conditions, poses a significant challenge for their further development. Notably, research has revealed that under a high degree of delithium, a portion of lattice oxygen undergoes oxidation, releasing oxygen that readily reacts with the electrolyte, leading to heat generation and thermal runaway, regardless of the short circuit inside the battery.[56,57] The high-valence transition metal ions are generally credited with contributing to the oxidation of lattice oxygen. As delithiation progresses, the valence state of TM ions elevates to TM^{4+}(e.g. Ni^{4+}, Co^{4+}), engaging in charge compensation of lattice oxygen oxidation through TM–O bonds, ultimately resulting in the reduction of TM ions and the oxidation of lattice oxygen.[12,58,59] Previously, it was widely accepted that in NCM materials, Mn can stay in the octahedral position of the TM layer, safeguarding the integrity of the layered structure and enhancing the thermal stability of the NCM cathode.[12] Noh et al studied the effect of Ni content on the thermal stability of NCM by DSC,[14] and discovered that as the increase of Ni content and the decrease of Mn content, the thermal stability of NCM cathode ($LiNi_xCo_yMn_zO_2$, x = 1/3, 0.5, 0.6, 0.7, 0.8 and 0.85) progressively diminishes under a fixed voltage. This is attributed to the improved thermal stability of Mn due to its electrochemical inertness. Consequently, numerous researchers aimed to boost Mn content to improve the thermal stability of the material. For example, Sun et al achieved this by constructing the core-shell structure of Mn-rich shell and Ni-rich core, significantly improving the electrochemical performance.[60]

However, Liu et al posited that the reduction of Ni content and its impact on the improving of thermal stability were overlooked.[61] Furthermore, as shown in Figure 4b–d, Liu et al observed that the Co rich material released less oxygen and had a higher phase transition temperature during the cycle by maintaining Ni content while altering the Mn/Co ratio. This indicates that Co plays a pivotal role in enhancing the thermal stability of the material under deep delithiation states. Through linear combination fitting (LCF) of XAS spectra, it was discovered that Co is consistently reduced before Ni, which favors tetrahedral coordination and contributes to improved thermal stability as demonstrated by the calculation of crystal field stabilization energy (CFSE) and the evidence of XAS spectra. During the phase transformation, the transition metal (TM) cations pass from a face-sharing tetrahedral site to an adjacent octahedral lithium vacant site. Their preference for specific sites is the crucial factor determining their migration behaviors, which is influenced by their octahedral-site stabilization energy (OSSE).[31] According to crystal field theory, crystal field stabilization energy (CFSE) is believed to calculate and compare the octahedral and tetrahedral site preferences. For instance, as shown in Table 1, $Co^{4+}$with d^5 electrons has an OSSE of 0, indicating that migration of Co^{4+}in tetrahedral sites is energetically favorable, which in turn hinders Ni migration.[62]

As shown in Figure 4a, during the phase transition, the TM cation traverses through a cohedral tetrahedral site to occupy the adjacent octahedral lithium vacancy. It can be delineated

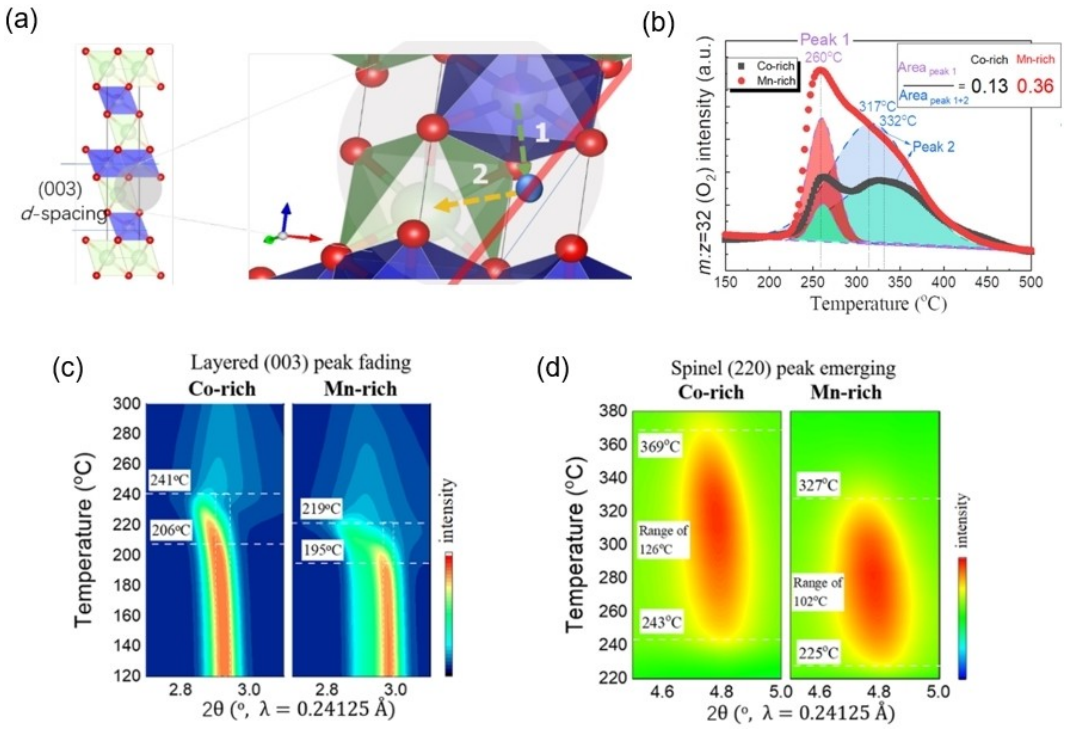

Figure 4. (a) Illustration of the impeding effect of Cobalt in occupying the tetrahedra site that blocks nickel migration. (b) Operando oxygen outgassing and phase transformation of Ni-rich layered $Li_{0.1}Ni_{0.83}Co_{0.11}Mn_{0.06}O_2$ and $Li_{0.1}Ni_{0.83}Co_{0.06}Mn_{0.11}O_2$ cathodes. The contour plots of the (c) layered (003) diffraction peak fading and (d) spinel (220) peak emerging during heating of Co-rich and Mn-rich cathode.[61] Copyright (2020) American Chemical Society.

Table 1. The OSSE of different transition metal cations.

Ion	Octahedral CFSE[a]	Tetrahedral CFSE[b]	Octahedral-site stabilization energy (OSSE)[c]
Ni^{4+}: d^6	$t_{2g}^6e_g^0$: −12/5 Δo	$e_g^3t_{2g}^3$: −3/5 Δt	−2.13 Δo
Co^{4+}: d^5	$t_{2g}^5e_g^0$: 0 Δo	$e_g^3t_{2g}^2$: 0 Δt	0
Mn^{4+}: d^3	$t_{2g}^3e_g^0$: −6/5 Δo	$e_g^2t_{2g}^1$: −4/5 Δt	−0.848 Δo
Ni^{3+}: d^7	$t_{2g}^3e_g^0$: −1.88 Δo	$e_g^2t_{2g}^1$: −0.53 Δt	−1.35 Δo
Co^{3+}: d^6	$t_{2g}^3e_g^0$: −2.4 Δo	$e_g^2t_{2g}^1$: −0.27 Δt	−2.13 Δo
Mn^{3+}: d^4	$t_{2g}^3e_g^0$: −0.6 Δo	$e_g^2t_{2g}^1$: −0.18 Δt	−0.42 Δo

into two steps. In step one, the TM ions move from the transition metal layer octahedral position through the face-sharing plane to the tetrahedral position in the middle of the Li octahedral position. Subsequently, the TM ions leap from the common-sided tetrahedral position to the Li octahedral position. Given the preferential tetrahedral occupancy of Co compared to Ni and Mn, Co occupies the cohedral tetrahedral position prior to Ni, thereby impeding the migration of Ni. This obstruction in turn hinders the transformation of mesoid spinel phase and the oxidation of lattice oxygen during the cycle. Conversely, Mn shows electrochemical inertia in the material, not hindering Ni migration, thus significantly diminishing the thermal stability of the material.

2.3. Cobalt-Lean/Free Nickel-based Layered Transition Metal Oxides

While Cobalt plays a crucial role in Nickel-based layered transition metal oxides, its classification as a precious metal has constrained the broader commercial utilization of these materials.[63] In addition, due to its uneven distribution and vulnerability to global events, Co is perceived as one of the most significant risk factors in the electric vehicle supply chain.

Figure 5a shows drastic fluctuations of Cobalt price on the London Metal Exchange (LME) since 2015. It is evident that the price of Cobalt exhibits high volatility. Even a lack of sulfuric acid supply for Cobalt extraction can also affect the price hike. Moreover, the Democratic Republic of Congo accounts for half of the world's Cobalt resources, compared with China, the largest manufacturer of lithium batteries, which accounts for only about 1% of the total reserves (Figure 5b). In addition, Co mining there is vulnerable to local political instability and often involves the ethical issue of child labor, which significantly raises concerns about the reliable supply of Cobalt.[64]

Tesla has announced plans to develop and utilize cathode materials with a Cobalt content of less than 3% in lithium-ion batteries (LIBs) for electric vehicles. They have been extensively collaborating with leading battery manufacturers to pursue the ultimate objective of eliminating Cobalt from LIBs. Consequently, "Cobalt-free" cathodes have attracted significant attention since then. However, the practical application of those is still challenging. On the one hand, the reduction of Cobalt will increase the mixing of cations, thereby reducing the structural stability during cycling. On the other hand, the absence of Cobalt will also exacerbate the phase transition of the material during the cycle, which may trigger thermal runaway.[65] Through the study of the action mechanism of Cobalt in Nickel-based Layered transition metal oxide materials, more strategies for the substitution of Cobalt may be proposed.

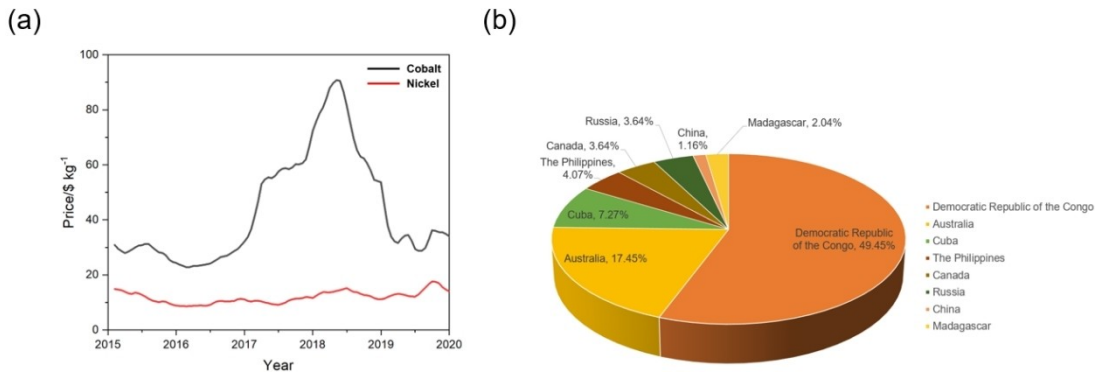

Figure 5. (a) Global market price of Cobalt and nickel raw materials from Jan. 2015 to Jan. 2020 from London Metal Exchange. (b) The global distribution of Cobalt reserves.

3. Modification Methods for the Elimination of Cobalt in the Nickel-based Layered Transition Metal Oxides

This review encapsulates the contemporary strategies for modifying Co-free Nickel-based layered transition metal oxide cathodes. Notably, some substituents without unpaired electrons in the outer layer can also form a weak 180° superexchange configuration with Ni^{2+} ions in an inverse orientation, thereby mitigating cation mixing. Given the magnetic reluctance effect, it is advisable to select substituents without unpaired electrons in the outer layer and without magnetic moments, such as Mg^{2+}, Al^{3+}, Ti^{4+}, Zr^{4+}. Furthermore, Co^{3+} occupies the tetrahedral position between the transition metal layer octahedron and the Li octahedron, preceding Ni^{2+} during the delithiation process to prevent the migration of Ni. Consequently, substituents with a preference for tetrahedral positions, like B^{3+}, can be selected to partially replace Co's role.

On the other hand, the absence of Cobalt will aggravate the release of lattice oxygen, which may have side reactions with the electrolyte, thus resulting in the thermal runaway of the batteries. By establishing a protective layer on the surface, surface coating can mitigate the side reactions at the interface, including the side reactions between oxygen and electrolyte, or between electrolyte and surface cathode materials.[66–70] Moreover, certain coating layers are conducive to establishing robust metal-oxygen bonding with lattice oxygen in the positive electrode material, enhancing lattice oxygen stability.[71,72]

3.1. Cation Ion Doping

3.1.1. Single Element Doping

Currently, numerous researchers are exploring ways to mitigate the Li/Ni mixing degree in the positive electrode of Nickel-based layered transition metal oxides by adding single ionic substituents without outer layers of unpaired electrons.[73–77] As exemplified in Figure 6a, Sun et al achieved uniform Ti doping in the precursor of NCM811 through a hydrolysis process.[78] Consequently, the cationic mixing degree of doped cathode material was significantly inhibited (from 6.76% to 3.13%), leading the improvement of discharge capacity from 188 mAh/g to 196 mAh/g at 0.5 C and long-term cyclability. Moreover, Li et al enhanced the electrochemical properties of $LiNi_{0.5}Mn_{0.5}O_2$ by incorporating 1 atom% Mo.[79] As shown in Figure 6c, comparison of the STEM images of undoped and Mo-doped LNMO particles before cycling reveals that atomic column in the Li layer of undoped LNMO is intensified compared to Mo-

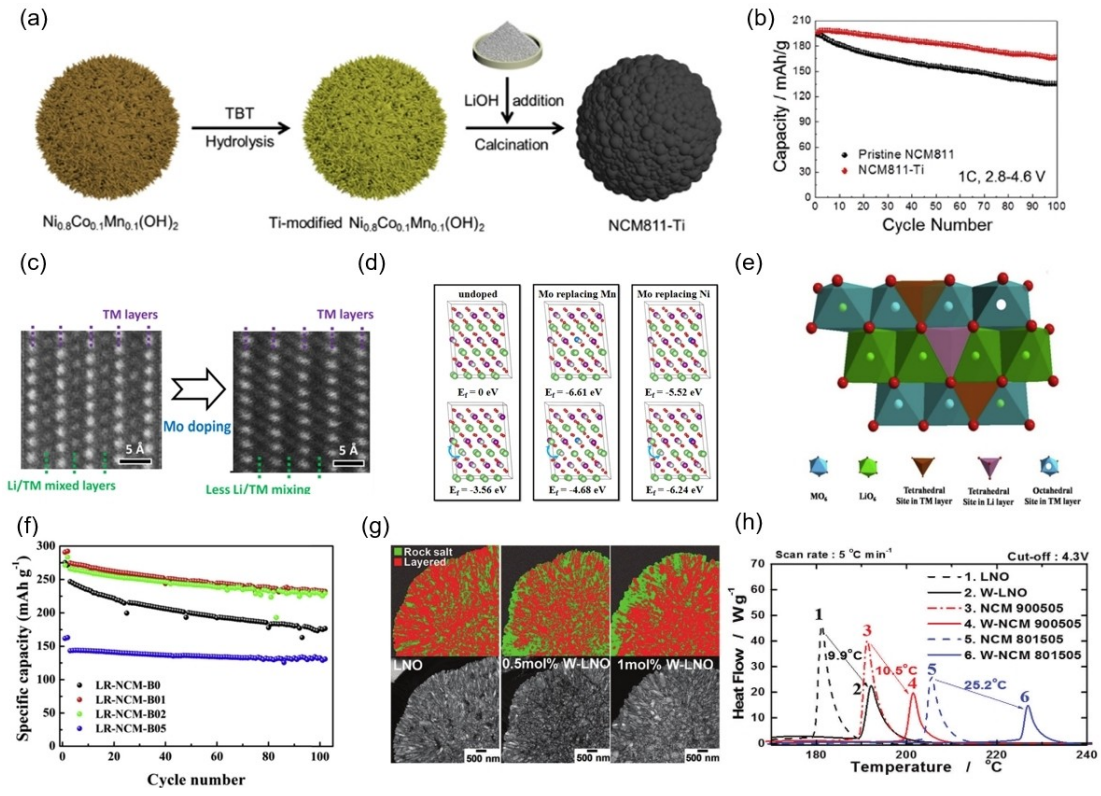

Figure 6. (a) Schematic illustrates the synthesis process of Ti-doped $LiNi_{0.8}Co_{0.1}Mn_{0.1}O_2$ (NCM811-Ti). (b) Cycling performance for pristine NCM811 and NCM811-Ti tested at 1 C (1 C = 200 mA/g).[78] Copyright (2019) Elsevier. (c) HAADF STEM image of a near-surface region in undoped LNMO and Mo-doped LNMO. (d) DFT calculations of undoped and Mo-doped LNMO structures.[79] Copyright (2019) American Chemical Society. (e) The crystal structure of Li-rich-NCM. (f) Cycling performance of the $Li(Li_{0.2}Ni_{0.13}Co_{0.13}Mn_{0.54})_{1-x}B_xO_2$ samples at 55 °C at 0.5 C after activation at 0.2 C between 2.0 V and 4.6 V.[80] Copyright (2016) Elsevier. (g) ASTAR TEM phase mapping and corresponding bright field images for LNO, 0.5 mol% and 1 mol% W-LNO, showing distribution of the rocksalt phase in the respective cathode. (h) DSC results of the pristine, W-doped layered cathode materials.[81] Copyright (2018) Royal Society of Chemistry.

doped LNMO. The results indicate that the doping of Mo inhibits cationic mixing in the Li and transition metal layers because Ni, Mn and Mo atoms are more distinguishable from lighter substances. In particularly, DFT calculation (Figure 6d) reveals that when Mo occupies the Mn position, the configuration without cationic mixing exhibits greater stability than after the one with cationic mixing, which is the energic driving force for the reduced cation mixing induced by Mo doping in LNMO. By summarizing the Bader charge analysis results for the three simulated structures without cation mixing, they found that the charge values of some Ni atoms near the Mo dopant were significantly higher, which hinder Li/Ni mixing because of the smaller ionic radius of Ni^{3+}(0.56 Å) as compared to that of Ni^{2+}or Li^{+}(0.69 and 0.76 Å, respectively). In contrast, the Bader charge values of all of the Mn atoms in both doped structures were slightly reduced compared to undoped LNMO. The Coulombic interaction is altered by such Mo-induced charge redistribution, which introduces localized structure distortions, thus dramatically affecting the system's formation energy. In comparison to the original LNMO, LNMO doped with Mo demonstrated enhanced cyclability, showing an increased capacity retention rate from 48.4% to 59.0% after 100 cycles. Furthermore, doping with ions that prefer tetrahedral sites can effectively inhibit the migration of Ni^{2+}during delithiation, thus stabilizing the lattice oxygen. Pan et al demonstrated that the stable crystal structure of boron-doped lithium rich layered oxides is attributed to the fact that the boron in the tetrahedral site, which prevents the migration of TM ions (Figure 6e).[51] As previous reported,[80] the TM ions migrate to tetrahedral sites through oxygen vacancies, and from there, they can migrate to other sites. Upon B^{3+}doping, B^{3+}occupying the tetrahedral position obstructs the migration of TM ions, thus greatly improving the initial discharge capacity and capacity retention rate, for instance, the 1 mol% boron-bound sample can deliver a capacity retention of 89.9% after 50 cycles at 0.2 C, which is much higher than that of the undoped sample with a capacity retention rate of 79.2%. Nonetheless, an excessive boron doping level of 5 mol% resulted in a significant decrease in the material's specific capacity, which should be mainly attributed to increase of the particle size and the migration path of lithium ions upon excessive doping of B^{3+}(Figure 6f).

Rather than occupy position substitution, incorporation with elements that form robust metal-oxygen bonding with lattice oxygen can alleviate the effect of Cobalt loss on the stability of lattice oxygen. Kim et al indicated that doping of W can elevates the surface energy of layered LNO,[81] while decreasing the surface energy of rock salt $LiNiO_2$ (LNO). As the W doping content rises, a greater amount of rock salt phase segregates on the surface, and the computed oxygen release energy of the rock salt phase surpasses both the doped and undoped W layered phases (Figure 6g). Consequently, the introduction of W enhances the chemical stability of the cathode surface by inhibiting oxygen release, thereby alleviating the capacity attenuation and improving the thermal stability observed for un-doped LNO cathodes (Figure 6h).

Currently, single-ion doping usually replaces Cobalt to some extent in Nickel-based Layered transition metal oxide materials, such as reducing cationic mixing or inhibiting lattice oxygen release. However, it could rarely solve all the problems caused by the elimination of Cobalt.

3.1.2. Multi-Element Doping

Through a variety of ions doping cathode materials, multi-ion doping sometimes shows even better performance with the help of synergistic effects.[15,82,83] In this respect, most experiments on multi-ion doping involve two individual ions that produce different effects, which complement each other to improve the comprehensive performance of materials.[84–88]

Al/Mg co-doping is proposed by Woo et al,[89] while the doped Al^{3+}no unpaired electrons in the outermost layer like $Co^{3+}$is distributed in the transition metal layer to weaken the super-exchange structure formed by antiposition $Ni^{2+}$and Mg^{2+} is preferentially located in the Li layer to reduce the total amount of Ni^{2+}occupied in the Li layer, which results in the doping of Al^{3+}or Mg^{2+}alone being able to significantly reduce the Li/Ni mixing (Figure 7a). Moreover, the higher bonding strength between Mg and Al ions with oxygen compared to Ni–O contributes to stabilizing lattice oxygen, significantly improving the thermal stability of NCM (Figure 7b). As shown in Figure 7c, when both Al and Mg were doped with 1 mol% each, the capacity retention rate reached 92% and the initial discharge capacity of 191 mAh/g was higher than that of the single doped sample. Lv et al crafted a Nickel-rich Cobalt-free cathode material modified with dual elements of In and Sn ($InSn\text{-}LiNi_{0.85}Mn_{0.09}Al_{0.06}O_2$,[90] InSn-NMA85) through a streamlined one-step sintering method (Figure 7e). Given a large ionic radius and a high valence state, Sn^{4+}can adeptly adjust lattice parameters and mitigates the lattice contraction in the c direction at a highly charged state, thereby reducing the lithium ion diffusion barrier and improving the lithium ion diffusion efficiency, as well as inhibiting Nickel ion migration and reducing oxygen release. Furthermore, this craft forms a $LiInO_2$ coating on the particle surface, safeguarding the NMA85 particles from excessive cathode/electrolyte interface side reactions during cycling. As shown in Figure 7d, benefited from the dual ionic doping, the modified material maintained a capacity retention rate of nearly 100% after 100 cycles at 0.5 C, compared with only 90% of the original NMA85 material within the voltage range of 2.7–4.5 V at 30 °C.

Beyond common two-element doping, some researchers have ventured into employing high-entropy doping strategies to mitigate the negative effect of Co elimination.[91,92] The essence of this high-entropy strategy lies in maximizing the allocation entropy through the integration of multiple primary elements, thereby enhancing the stability of cathode materials.[93] Zhang et al achieved this by doping Ti, Mg, Nb and Mo four elements into Cobalt-free LNMO cathode materials,[94] resulting in a $LiNi_{0.8}Mn_{0.13}Ti_{0.02}Mg_{0.02}Nb_{0.01}Mo_{0.02}O_2$ (HE-LNMO) cathode material with high thermal stability significantly surpassing NCM-811 and comparable with NMC532 with a much lower Ni content (Figure 7g). Remarkably, this material demonstrates an unprecedented zero volume change during

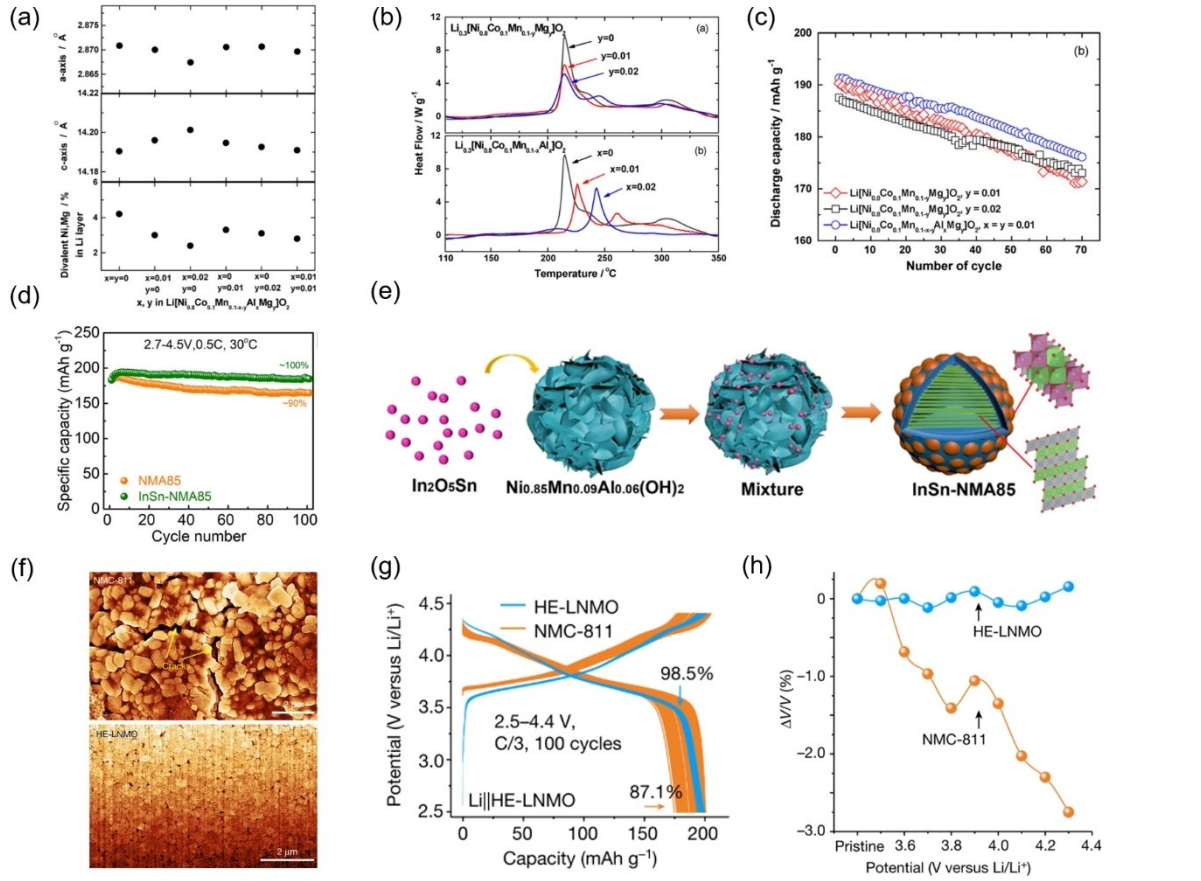

Figure 7. (a) Variation of the structural parameters obtained from the Rietveld refinements of the XRD data of $Li[Ni_{0.8}Co_{0.1}Mn_{0.1-x-y}Al_xMg_y]O_2$. (b) Differential scanning calorimetry (DSC) traces of $Li[Ni_{0.8}Co_{0.1}Mn_{0.1-y}Mg_y]O_2$ and $Li[Ni_{0.8}Co_{0.1}Mn_{0.1-x}Al_x]O_2$ charged to 4.3 V at a scan rate of 5 °C min^{-1}. (c) Variation of discharge capacities of $Li/Li[Ni_{0.8}Co_{0.1}Mn_{0.1-x-y}Al_xMg_y]O_2$ cells as a function of cycle number cycled in the range of 3.0–4.3 V at a 0.5 C-rate (100 mA/g).[89] Copyright (2009) Elsevier. (d) Cycling performance of the NMA85 and InSn-NMA85 cathodes at 30 °C. (e) Schematic illustration of the synthesis route of the InSn-NMA85.[90] Copyright (2023) Elsevier. (f) Representative SEM cross-section images of NMC-811 (upper panel) and HE-LNMO (lower panel) secondary particles. (g) Long-cycle charge-discharge profiles of the half cells containing HE-LNMO and NMC-811, within 2.5–4.5 V (versus Li/Li$^+$). (h) Volume change of HE-LNMO in comparison with NMC-811 during the first charge, within 3.0–4.3 V (versus Li/Li$^+$).[94] Copyright (2022) Springer Nature.

Li$^+$intercalation and deintercalation (Figure 7h), while maintaining zero strain without inducing excessive cracks after long cycles (Figure 7f). Consequently, the improved material shows a significantly improved capacity retention rate (85% at 1,000 cycles in half cell) compared to commercial $LiNi_{0.8}Mn_{0.1}Co_{0.1}O_2$ (NMC-811).

Some significant progress has been made in the substitution of Cobalt in Nickel-based layered transition metal oxides and there is no doubt that ion-doping plays an irreplaceable role in this process. Moreover, the optimization of doping amount and depth is significant, as well as more combinations of different elements. However, ion doping does not effectively address surface side reactions, thus combining with other modification strategies may lead to better optimization goals.

3.2. Surface Coating

For Nickel-based layered transition metal oxides, the elimination of Cobalt intensifies the release of oxygen from the lattice and the reaction between oxygen and electrolyte is the primary cause of battery thermal runaway during cycling.[12,95] Furthermore, the side reactions occurring at the interface and HF corrosion generated in electrolytes are significant contributors to capacity degradation and safety concerns.[96–98] Surface coating has emerged as an efficient approach to inhibit these side reactions.[66,67] Along with hindering the reaction of oxygen with the electrolyte,[99,100] ions in the coating layer establish robust metal-oxygen bonds with oxygen in the TM layers, thereby modulating oxygen activity and suppressing the liberation of lattice oxygen.[101–103]

As proposed by Lin et al,[104] a large number of nano-sized aluminum fluoride particles were distributed on the surface of $LiNi_{0.5}Mn_{0.5}O_2$ particles, to form the AlF_3 coating layer (Figure 8a). As depicted in Figure 8b, the AlF_3-coated material exhibited a noteworthy resilience in its initial discharge capacity, retaining a value of 174.2 mAh/g, comparable to the uncoated sample. Remarkably, after 50 cycles, the capacity retention rate underwent a significant enhancement, attaining 87.9%, surpassing the original material's 72.3%. Wu et al proposed a surface modification strategy of doping $Li_{1.2}Ni_{0.32}Mn_{0.48}O_2$ with Ta^{5+},[105] that is, Ta^{5+}ions occupy the lithium site in the surface lattice

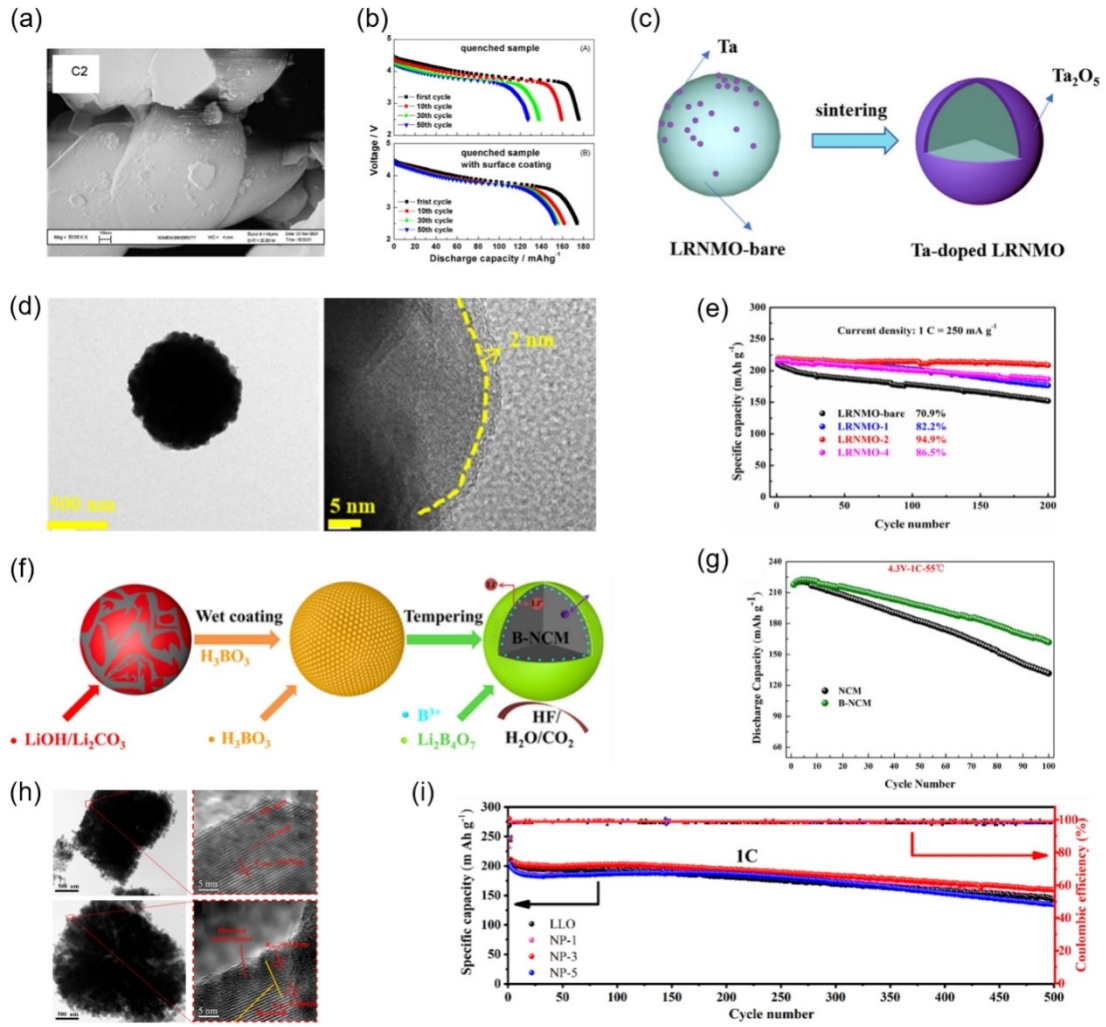

Figure 8. (a) Quenched sample with surface coating. Magnification of samples are 50 k. (b) Discharge profiles of $Li/LiNi_{0.5}Mn_{0.5}O_2$ cells with/without AlF_3 coating at various cycles at 28 mA/g (0.1 C) in the voltage range of 2.5–4.5 V.[104] Copyright (2010) Elsevier. (c) Schematic diagram of the synthesis of Ta-modified materials. (d) The SEM images of LRNMO coated by Ta_2O_5. (e) Testing LRNMO with/without Ta_2O_5 for 200 cycles with current density of 1 C.[105] Copyright (2022) Elsevier. (f) Schematic diagram of $LiNi_{0.925}Co_{0.03}Mn_{0.045}O_2$ cathode material modified with $Li_2B_4O_7$ and B^{3+}. (g) Electrochemical performance of both samples in range of 2.8–4.3 V at 25 °C.[107] Copyright (2022) Elsevier. (h) TEM and HRTEM images of Co-free LLOs and NP-3, respectively. (i) Discharge capacity at 1 C for the Co-free LLOs, NP-1, NP-3, and NP-5 cathode materials.[108] Copyright (2022) American Chemical Society.

structure of LRNMO to form the 2 nm Ta_2O_5 coating layer (LRNMO-2 sample, Figure 8d). The robust bond cooperation between Ta–O serves to consolidate the surface structure, stabilizing the migration of reactive oxygen species, thereby enhancing the material's cyclic stability. With a high initial capacity of 220 mAh/g (Figure 8e), the LRNMO-2 sample can deliver a capacity retention of 94.9% after 200 cycles, which was much higher than 70.9% of LRNMO bare electrode. This underscores the excellent maintenance of the layered structure of the LRNMO-2 electrode during cycling, effectively inhibiting the layered-to-spinel phase transition.

Furthermore, more complex coating strategies have been reported to eliminate the effects of Cobalt deficiency.[106–110] Luo et al have explored a combination of doping and coating modification on NCM cathode by doping $B^{3+}$and coating with $Li_2B_4O_7$.[107] The small B^{3+}ions block the migration pathways of transition metal ions and preserve oxygen vacancies by occupying the tetrahedral voids, stabilizing the crystal structure of Li-rich layered oxides. Meanwhile, the coating layer of the surface mitigates the side reaction of the cathode/electrolyte interface, thereby improving the cyclic performance of the material.[107] As shown in Figure 8g, the modified sample showed excellent cycle retention at 1 C and 55 °C, which was 72.86% after 100 cycles, while the bare NCM retained only 59.65%. Chang et al successfully prepared spinel coating Cobalt-free lithium rich layered oxides doped with phosphate by co-treating with weak acidity and weak alkali ($NH_4H_2PO_4$ solution) (Figure 8h).[108] The spinel coating promotes the migration of Li^+ and suppresses O_2 release by stabilizing the surface structure,[107] while the doping of PO_4^{3-} hinders the migration of transition metal ions between oxygen octahedral and tetrahedral sites, enhancing the material's structural stability during charge-discharge cycles and inhibiting the transition from the layered to spinel phase. Benefited from the

combination strategy, the material with 3% $NH_4H_2PO_4$ provides a high discharge capacity of 211.5 mAh/g at 1 C and a capacity retention of 75% even 500 cycles (Figure 8i), which is much higher than the undoped Co-free LLO material (capacity retention rate of 65%).

As shown in Table 2, based on the properties of the coating materials, the inactive coating materials (such as AlF_3) act as a physical protective layer and reduce the side reactions between cathode materials and electrolytes. However, owing to its poor ionic and electronic conductive, the C-rate performance is unsatisfactory. The Li^+/electron conductive coating materials (such as Li_2SnO_3, $Li_2B_4O_7$) not only own favorable electrochemical stability akin to inactive coating materials but also facilitate enhanced ionic or electronic transfer at the cathode interface, thereby achieving superior rate capability. Compared with inactive coating materials, however, the deposition of Li^+/electron conductive coating layer is generally more complicated. So, it is still a challenge to prepare a continuous and uniform Li^+/electron conductive coating layer.

4. Summary and Perspective

The scarcity of Cobalt in the Earth's crust and its supply risks have hindered the further advancement of Nickel-based layered transition metal oxide in the battery industry. Nonetheless, the absence of Cobalt poses significant challenges to the structural stability and safety of these materials. The implementation of strategies such as surface coating and cation ion doping has played a pivotal role in enhancing the battery performance of the Cobalt-free Nickel-based layered transition metal oxide materials (Figure 9).

Doping is an effective method to stabilize the crystal structure and minimizing the cation mixing. Substituting elements like Zr, Ti, Mg, and Al into the lattice can stabilize the interaction with oxygen atoms, maintain the layered structure and improve the thermal stability, while inhibiting the cation mixing by reducing the super-exchange structure formed with the inverse Ni. Doping ions with tetrahedral preference such as $B^{3+}$and PO_4^{3-} is an effective method to inhibit the migration of transition metal ions, thereby stabilizing the material structure during cycling. Particularly, the combination of multiple options provides synergies resulting in superior cycle performance. However, elemental doping has no apparent effect on inhibiting electrolyte corrosion and decomposition or reducing the interface resistance of the batteries. In addition, since electrochemical reactions mainly occur at the electrode/electrolyte interface, the surface properties of materials are paramount in determining their electrochemical behavior. In this regarding, surface coating is serves as a crucial strategy to safeguard surfaces from electrolyte reactions and HF corrosion generated in electrolytes. Proper surface coating can inhibit the oxidation of lattice oxygen, thereby enhancing the structural stability of the material. However, the surface coating cannot fundamentally inhibit structural transformation in the bulk of Co-free Ni-rich layered materials.

In the future, the uniform doping effect and precising control of doping sites will be the direction of further research. Due to the tiny amounts of the doping elements in the Ni-rich cathode materials, it is critically important to homogeneously

Table 2. Different modification methods for the elimination of Cobalt in the Nickel-based layered transition metal oxides.

No.	Cathode materials	Strategies	Initial Capacity (0.1 C)/ mAh/g	Cycling performance improvement	Rate performance improvement mAh/g	Ref.
1	NCM811	Ti-doping	188 at 0.5 C (2.8–4.6 V)	84% vs. 70% at 1 C after 100 cycles	160 vs. 140 at 2 C	[74]
2	NM55	Mo-doping	178 (50 mA/g) (2–4.5 V)	59% vs. 48.4% (50 mA/g) after 100 cycles		[75]
3	NCM900505	W-doping	210 at 0.5 C (2.7–4.3 V)	95% vs. 88% at 0.5 C after 100 cycles		[77]
4	$LiNiO_2$	Mg, Ti-doping	175 at 1 C (2.5–4.4 V)	95% vs. 73.6% at 0.1 C after 50 cycles		[83]
5	NCM811	Al, Mg-doping	191 at 0.5 C (3–4.3 V)	92% vs. 82% at 0.5 C after 100 cycles		[85]
6	$LiNi_{0.85}Mn_{0.09}Al_{0.06}O_2$	In, Sn-doping	185 at 0.5 C (2.7–4.5 V)	100% vs. 90% at 0.5 C after 100 cycles	140 vs. 120 at 10 C	[86]
7	NM82	Ti, Mg, Nb, Mo-doping	180 at C/3 (2.5–4.3 V)	88% vs. 44% at C/3 after 400 cycles		[90]
8	NM55	AlF_3 coating	174.2 at 0.1 C (2.5–4.5 V)	87.9% vs. 72.3% at 0.1 C after 50 cycles		[100]
9	NM82	Li_2SnO_3 coating and Sn^{4+}doping	191.3 at 0.2 C (2.75–4.2 V)	90.54% vs. 81.23% at 0.2 C after 300 cycles	155.49 vs. 136.01 at 5 C	[102]
10	$LiNi_{0.925}Co_{0.03}Mn_{0.045}O_2$	$Li_2B_4O_7$ coating and B^{3+}doping	191.3 at 0.2 C (2.75–4.2 V)	72.86% vs. 59.65% at 0.2 C after 100 cycles	171.3 vs. 151.8 at 10 C	[103]
11	$Li_{1.2}Mn_{0.6}Ni_{0.2}O_2$	Spinel coating and PO_4^{3-} doping	211.5 at 1 C (2–4.8 V)	75% vs. 65% at 1 C after 500 cycles	160.1 vs. 133.4 at 5 C	[104]

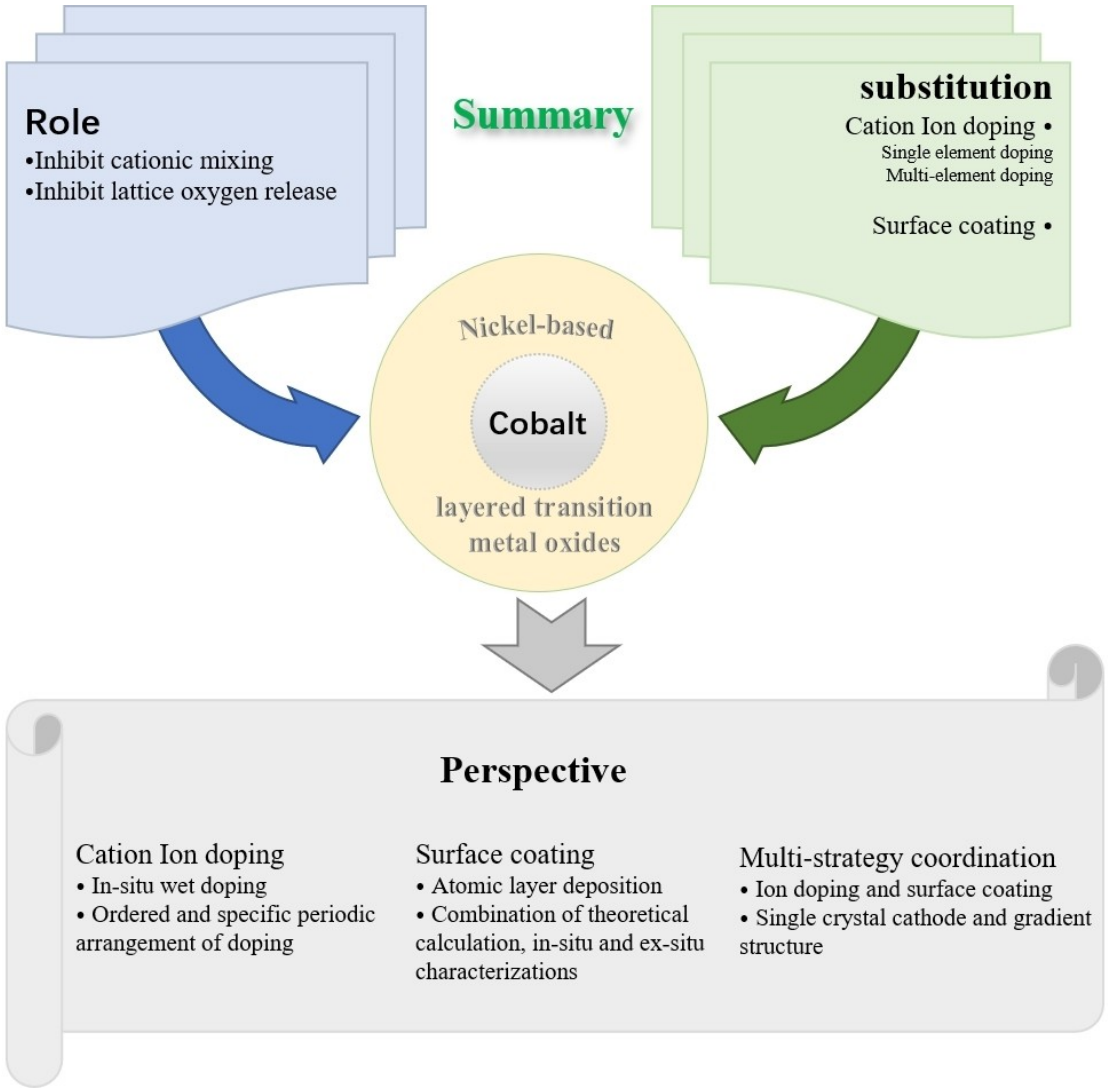

Figure 9. The role and substitution of Cobalt in the Nickel-based layered transition metal oxides and the challenge of the modification methods in the future.

distribute the doping elements into the crystal. By adding dopants during precursor synthesis and subsequent co-lithiation sintering process, in-situ wet doping can easily obtain the homogeneous distribution of dopants inside the particle, thus achieving a better electrochemical performance. In addition, with the advances of synthesis and characterization technology, how to control the ordered and specific periodic arrangement of doping ions are considered, which may be conducive to implement some special ideas, such as defect site doping and certain site doping. For surface coating, one challenge is how to prepare a uniform coating on the surface of cathode particles. Atomic layer deposition (ALD) is a promising technique to prepare the uniform coating on a small scale. Moreover, more detailed and comprehensive study are needed for a deeper understanding of the intrinsic mechanism of surface coating. The combination of theoretical calculation, in-situ and ex-situ characterizations is a promising approach.

Eliminating the effect of the absence of Co on the positive electrode of the Nickel-based layered transition metal oxide is a complex problem, which should be considered not only from the surface reaction, but also from the bulk structure. It may be difficult for a single strategy to play a critical role, thus multi-strategy coordination may be the direction to solve this problem.

Acknowledgements

The project was supported by the National Key R&D Program of China (2021YFB2400400), the National Natural Science Foundation of China (Grant No. 22379120), the Key Research and Development Plan of Shanxi Province (China, Grant No. 2021JLM-36), "Young Talent Support Plan" of Xi'an Jiaotong University (71211201010723), "Young Talent Support Plan" of Xi'an Jiaotong University (HG6J003), "1000-Plan program" of Shaanxi Province and the Higher Education Institution Academic Discipline Innovation and Talent Introduction Plan ("111 Plan")(No.B23025).

Conflict of Interests

The authors declare no conflict of interest.

Keywords: Nickel-based · Surface coating · Cationic mixing · Co-lean/free · Ion doping

[1] X.-G. Yang, T. Liu, C.-Y. Wang, *Nat. Energy* **2021**, *6*, 176–185.
[2] W. Li, E. M. Erickson, A. Manthiram, *Nat. Energy* **2020**, *5*, 26–34.
[3] Z. Wu, Y. Wang, X. Liu, C. Lv, Y. Li, D. Wei, Z. Liu, *Adv. Mater* **2019**, *31*, 1800716.
[4] F. Cerdas, P. Titscher, N. Bognar, R. Schmuch, M. Winter, A. Kwade, C. Herrmann, *Energies* **2018**, *11*, 150.
[5] D. Andre, S.-J. Kim, P. Lamp, S. F. Lux, F. Maglia, O. Paschos, B. Stiaszny, *J. Mater. Chem. A* **2015**, *3*, 6709–6732.
[6] M. S. Whittingham, *Chem. Rev* **2004**, *104*, 4271–4302.
[7] F. Schipper, P. K. Nayak, E. M. Erickson, S. F. Amalraj, O. Srur-Lavi, T. R. Penki, M. Talianker, J. Grinblat, H. Sclar, O. Breuer, *Inorganics* **2017**, *5*, 32.
[8] S.-T. Myung, F. Maglia, K.-J. Park, C. S. Yoon, P. Lamp, S.-J. Kim, Y.-K. Sun, *ACS Energy Lett.* **2017**, *2*, 196–223.
[9] Z. Liu, A. Yu, J. Y. Lee, *J. Power Sources* **1999**, *81*, 416–419.
[10] W. Li, S. Lee, A. Manthiram, *Adv. Mater* **2020**, *32*, 2002718.
[11] A. Aishova, G. T. Park, C. S. Yoon, Y. K. Sun, *Adv. Energy Mater.* **2020**, *10*, 1903179.
[12] K. W. Nam, S. M. Bak, E. Hu, X. Yu, Y. Zhou, X. Wang, L. Wu, Y. Zhu, K. Y. Chung, X. Q. Yang, *Adv. Funct. Mater.* **2013**, *23*, 1047–1063.
[13] N. Yabuuchi, T. Ohzuku, *J. Power Sources* **2003**, *119*, 171–174.
[14] H.-J. Noh, S. Youn, C. S. Yoon, Y.-K. Sun, *J. Power Sources* **2013**, *233*, 121–130.
[15] W. Yao, Y. Liu, D. Li, Q. Zhang, S. Zhong, H. Cheng, Z. Yan, *J. Phys. Chem. C* **2020**, *124*, 2346–2356.
[16] J. Zhang, X. Tan, L. Guo, Y. Jiang, S. Liu, H. Wang, X. Kang, W. Chu, *J. Alloys Compd.* **2019**, *771*, 42–50.
[17] A. Boulineau, L. Simonin, J.-F. Colin, C. Bourbon, S. Patoux, *Nano Lett.* **2013**, *13*, 3857–3863.
[18] M. Gu, I. Belharouak, J. M. Zheng, H. M. Wu, J. Xiao, A. Genc, K. Amine, S. Thevuthasan, D. R. Baer, J. G. Zhang, N. D. Browning, J. Liu, C. M. Wang, *ACS Nano* **2013**, *7*, 760–767.
[19] J. Zheng, M. Gu, J. Xiao, P. Zuo, C. Wang, J.-G. Zhang, *Nano Lett.* **2013**, *13*, 3824–3830.
[20] W. Liu, P. Oh, X. Liu, M. J. Lee, W. Cho, S. Chae, Y. Kim, J. Cho, *Angew. Chem. Int. Ed.* **2015**, *54*, 4440–4457.
[21] P. Rozier, J. M. Tarascon, *J. Electrochem. Soc.* **2015**, *162*, A2490–A2499.
[22] J. Zheng, Y. Ye, T. Liu, Y. Xiao, C. Wang, F. Wang, F. Pan, *Acc. Chem. Res.* **2019**, *52*, 2201–2209.
[23] J. Zheng, G. Teng, C. Xin, Z. Zhuo, J. Liu, Q. Li, Z. Hu, M. Xu, S. Yan, W. Yang, *J. Phys. Chem. Lett.* **2017**, *8*, 5537–5542.
[24] Y. Shen, X. Yao, S. Wang, D. Zhang, D. Yin, L. Wang, Y. Cheng, *ACS Appl. Mater.* **2021**, *13*, 58871–58884.
[25] S. J. Wachs, C. Behling, J. Ranninger, J. Moeller, K. J. J. Mayrhofer, B. B. Berkes, *ACS Appl. Mater.* **2021**, *13*, 33075–33082.
[26] D. Wang, C. Xin, M. Zhang, J. Bai, J. Zheng, R. Kou, J. Y. P. Ko, A. Huq, G. Zhong, C.-J. Sun, Y. Yang, Z. Chen, Y. Xiao, K. Amine, F. Pan, F. Wang, *Chem. Mater.* **2019**, *31*, 2731–2740.
[27] Y. Xiao, T. Liu, J. Liu, L. He, J. Chen, J. Zhang, P. Luo, H. Lu, R. Wang, W. Zhu, Z. Hu, G. Teng, C. Xin, J. Zheng, T. Liang, F. Wang, Y. Chen, Q. Huang, F. Pan, H. Chen, *Nano Energy* **2018**, *49*, 77–85.
[28] G. Wannier, *Phys. Rev. B* **1973**, *7*, 5017.
[29] N. Yabuuchi, Y. T. Kim, H. H. Li, Y. Shao-Horn, *Chem. Mater* **2008**, *20*, 4936–4951.
[30] S. M. Bak, E. Y. Hu, Y. N. Zhou, X. Q. Yu, S. D. Senanayake, S. J. Cho, K. B. Kim, K. Y. Chung, X. Q. Yang, K. W. Nam, *ACS Appl. Mater.* **2014**, *6*, 22594–22601.
[31] A. Manthiram, *Nat. Commun.* **2020**, *11*, 1550.
[32] S. Zhong, M. Lai, W. Yao, Z. Li, *Electrochim. Acta* **2016**, *212*, 343–351.
[33] J. Bréger, Y. S. Meng, Y. Hinuma, S. Kumar, K. Kang, Y. Shao-Horn, G. Ceder, C. P. Grey, *Chem. Mater.* **2006**, *18*, 4768–4781.
[34] Y. Hinuma, Y. S. Meng, K. Kang, G. Ceder, *Chem. Mater.* **2007**, *19*, 1790–1800.
[35] H. H. Li, N. Yabuuchi, Y. S. Meng, S. Kumar, J. Breger, C. P. Grey, Y. Shao-Horn, *Chem. Mater.* **2007**, *19*, 2551–2565.
[36] F. Lian, P. Axmann, C. Stinner, Q. Liu, M. Wohlfahrt-Mehrens, *J. Appl. Electrochem.* **2008**, *38*, 613–617.
[37] H. Chen, J. A. Dawson, J. H. Harding, *J. Mater. Chem. A* **2014**, *2*, 7988–7996.
[38] K. S. Kang, Y. S. Meng, J. Bréger, C. P. Grey, G. Ceder, *Science* **2006**, *311*, 977–980.
[39] H. Yu, Y. Qian, M. Otani, D. Tang, S. Guo, Y. Zhu, H. Zhou, *Energy Environ. Sci.* **2014**, *7*, 1068–1078.
[40] P. Yan, A. Nie, J. Zheng, Y. Zhou, D. Lu, X. Zhang, R. Xu, I. Belharouak, X. Zu, J. Xiao, *Nano Lett.* **2015**, *15*, 514–522.
[41] P. Yan, J. Zheng, D. Lv, Y. Wei, J. Zheng, Z. Wang, S. Kuppan, J. Yu, L. Luo, D. Edwards, M. Olszta, K. Amine, J. Liu, J. Xiao, F. Pan, G. Chen, J.-G. Zhang, C.-M. Wang, *Chem. Mater.* **2015**, *27*, 5393–5401.
[42] J. Zheng, T. Liu, Z. Hu, Y. Wei, X. Song, Y. Ren, W. Wang, M. Rao, Y. Lin, Z. Chen, *J. Am. Chem. Soc.* **2016**, *138*, 13326–13334.
[43] A. Van der Ven, G. Ceder, *Electrochem. Solid St.* **2000**, *3*, 301.
[44] J. Reed, G. Ceder, *Electrochem. Solid St.* **2002**, *5*, A145.
[45] Y. Kim, D. Kim, S. Kang, *Chem. Mater.* **2011**, *23*, 5388–5397.
[46] P. Yan, J. Zheng, J.-G. Zhang, C. Wang, *Nano Lett.* **2017**, *17*, 3946–3951.
[47] J. Kanamori, *J. Phys. Chem. Solids* **1959**, *10*, 87–98.
[48] P. Selwood, *J. Am. Chem. Soc.* **1964**, *86*, 1273–1273.
[49] N. A. Chemova, M. Ma, J. Xiao, M. S. Whittingham, J. Breger, C. P. Grey, *Chem. Mater.* **2007**, *19*, 4682–4693.
[50] N. A. Chernova, M. Ma, J. Xiao, M. S. Whittingham, J. Breger, C. P. Grey, *Chem. Mater.* **2007**, *19*, 4682–4693.
[51] M. Li, J. Lu, *Science* **2020**, *367*, 979–980.
[52] C. Lacroix, P. Mendels, F. Mila, Introduction to frustrated magnetism: materials, experiments, theory. Springer Science & Business Media 2011.
[53] Y. Taguchi, Y. Oohara, H. Yoshizawa, N. Nagaosa, Y. Tokura, *Science* **2001**, *291*, 2573–2576.
[54] J. Zhao, W. Zhang, A. Huq, S. T. Misture, B. Zhang, S. Guo, L. Wu, Y. Zhu, Z. Chen, K. Amine, F. Pan, J. Bai, F. Wang, *Adv. Energy Mater.* **2017**, *7*, 1601266.
[55] C. Delmas, M. Ménétrier, L. Croguennec, I. Saadoune, A. Rougier, C. Pouillerie, G. Prado, M. Grüne, L. Fournès, *Electrochim. Acta* **1999**, *45*, 243–253.
[56] X. Feng, M. Ouyang, X. Liu, L. Lu, Y. Xia, X. He, *Energy Storage Mater.* **2018**, *10*, 246–267.
[57] X. Liu, D. Ren, H. Hsu, X. Feng, G.-L. Xu, M. Zhuang, H. Gao, L. Lu, X. Han, Z. Chu, *JOULE* **2018**, *2*, 2047–2064.
[58] B. Seong-Min, H. Enyuan, Z. Yongning, Y. Xiqian, C. Sung-Jin, K. Kwang-Bum, C. K. Yoon, Y. Xiao-Qing, N. Kyung-Wan, *ACS Appl. Mater. Interfaces* **2014**, *6*, 22594–22601.
[59] E. Lee, S. Muhammad, T. Kim, H. Kim, W. Lee, W. S. Yoon, *Adv. Sci.* **2020**, *7*, 1902413.
[60] Y.-K. Sun, S.-T. Myung, M.-H. Kim, J. Prakash, K. Amine, *J. Am. Chem. Soc.* **2005**, *127*, 13411–13418.
[61] X. Liu, G.-L. Xu, L. Yin, I. Hwang, Y. Li, L. Lu, W. Xu, X. Zhang, Y. Chen, Y. Ren, C.-J. Sun, Z. Chen, M. Ouyang, K. Amine, *J. Am. Chem. Soc.* **2020**, *142*, 19745–19753.
[62] S. Choi, A. Manthiram, *J. Electrochem. Soc.* **2002**, *149*, A1157–A1163.
[63] S. Venkatraman, Y. Shin, A. Manthiram, *Electrochem. Solid St.* **2003**, *6*, A9–A12.
[64] Y. Kim, W. M. Seong, A. Manthiram, *Energy Storage Mater.* **2021**, *34*, 250–259.
[65] N. Voronina, Y.-K. Sun, S.-T. Myung, *ACS Energy Lett.* **2020**, *5*, 1814–1824.
[66] H. Yang, H.-H. Wu, M. Ge, L. Li, Y. Yuan, Q. Yao, J. Chen, L. Xia, J. Zheng, Z. Chen, J. Duan, K. Kisslinger, X. C. Zeng, W.-K. Lee, Q. Zhang, J. Lu, *Adv. Funct. Mater.* **2019**, *29*, 1808825.
[67] L. Li, L. Fu, M. Li, C. Wang, Z. Zhao, S. Xie, H. Lin, X. Wu, H. Liu, L. Zhang, *J. Energy Chem.* **2022**, *71*, 588–594.
[68] B. J. Ryu, A. L. Lee, Y. J. Lee, K. C. Nam, *Bull. Korean Chem. Soc.* **2009**, *30*, 3089–3091.
[69] H. G. Song, Y. J. Park, *Mater. Res. Bull.* **2012**, *47*, 2843–2846.
[70] F. Wu, Q. Li, L. Bao, Y. Zheng, Y. Lu, Y. Su, J. Wang, S. Chen, R. Chen, J. Tian, *Electrochim. Acta* **2018**, *260*, 986–993.
[71] M. Yoshitake, S. Yagyu, T. Chikyow, *Int. J. Metals* **2014**, *2*, 120840.
[72] U.-H. Kim, D.-W. Jun, K.-J. Park, Q. Zhang, P. Kaghazchi, D. Aurbach, D. T. Major, G. Goobes, M. Dixit, N. Leifer, *Energy Environ. Sci.* **2018**, *11*, 1271–1279.
[73] Z. Li, Y. Li, M. Zhang, Z. W. Yin, L. Yin, S. Xu, C. Zuo, R. Qi, H. Xue, J. Hu, *Adv. Energy Mater.* **2021**, *11*, 2101962.

[74] R. Tian, S. Yin, H. Zhang, D. Song, Y. Ma, L. Zhang, *Dalton Trans.* **2023**, *52*, 11716–11724.
[75] S. Muto, K. Tatsumi, Y. Kojima, H. Oka, H. Kondo, K. Horibuchi, Y. Ukyo, *J. Power Sources* **2012**, *205*, 449–455.
[76] L. Yeting, C. Xu, Q. Wenjiang, H. Bingxin, *J. Power Sources* **2020**, *450*, 961–969.
[77] F. Schipper, M. Dixit, D. Kovacheva, M. Talianker, O. Haik, J. Grinblat, E. M. Erickson, C. Ghanty, D. T. Major, B. Markovsky, D. Aurbach, *J. Mater. Chem. A* **2016**, *4*, 16073–16084.
[78] H. Sun, Z. Cao, T. Wang, R. Lin, Y. Li, X. Liu, L. Zhang, F. Lin, Y. Huang, W. Luo, *Mater. Today Energy* **2019**, *13*, 145–151.
[79] L. Li, J. Yu, D. Darbar, E. C. Self, D. Wang, J. Nanda, I. Bhattacharya, C. Wang, *ACS Energy Lett.* **2019**, *4*, 2540–2546.
[80] L. Pan, Y. Xia, B. Qiu, H. Zhao, H. Guo, K. Jia, Q. Gu, Z. Liu, *J. Power Sources* **2016**, *327*, 273–280.
[81] U. H. Kim, D. W. Jun, K. J. Park, Q. Zhang, P. Kaghazchi, D. Aurbach, D. T. Major, G. Goobes, M. Dixit, N. Leifer, C. M. Wang, P. Yan, D. Ahn, K. H. Kim, C. S. Yoon, Y. K. Sun, *Energy Environ. Sci.* **2018**, *11*, 1271–1279.
[82] M.-H. Kim, H.-S. Shin, D. Shin, Y.-K. Sun, *J. Power Sources* **2006**, *159*, 1328–1333.
[83] B. Zhang, L. Li, J. Zheng, *J. Alloys Compd.* **2012**, *520*, 190–194.
[84] W. Li, S. Lee, A. Manthiram, *Adv. Mater* **2020**, *32*, 2002718.
[85] N. Muralidharan, R. Essehli, R. P. Hermann, A. Parejiya, R. Amin, Y. Bai, Z. Du, I. Belharouak, *J. Power Sources* **2020**, *471*, 228389.
[86] N. Muralidharan, R. Essehli, R. P. Hermann, R. Amin, C. Jafta, J. Zhang, J. Liu, Z. Du, H. M. Meyer III, E. Self, *Adv. Mater* **2020**, *32*, 2002960.
[87] L. Mu, R. Zhang, W. H. Kan, Y. Zhang, L. Li, C. Kuai, B. Zydlewski, M. M. Rahman, C.-J. Sun, S. Sainio, *Chem. Mater* **2019**, *31*, 9769–9776.
[88] L. Mu, W. H. Kan, C. Kuai, Z. Yang, L. Li, C.-J. Sun, S. Sainio, M. Avdeev, D. Nordlund, F. Lin, *ACS Appl. Mater.* **2020**, *12*, 12874–12882.
[89] S. W. Woo, S. T. Myung, H. Bang, D. W. Kim, Y. K. Sun, *Electrochim. Acta* **2009**, *54*, 3851–3856.
[90] Y. Lv, S. Huang, S. Lu, T. Jia, Y. Liu, W. Ding, X. Yu, F. Kang, J. Zhang, Y. Cao, *Chem. Eng. J.* **2023**, *455*, 140652.
[91] C. Zhao, F. Ding, Y. Lu, L. Chen, Y. S. Hu, *Angew. Chem. Int. Ed.* **2020**, *59*, 264–269.
[92] Z. Lun, B. Ouyang, D.-H. Kwon, Y. Ha, E. E. Foley, T.-Y. Huang, Z. Cai, H. Kim, M. Balasubramanian, Y. Sun, *Nat. Mater.* **2021**, *20*, 214–221.
[93] J. W. Yeh, S. K. Chen, S. J. Lin, J. Y. Gan, T. S. Chin, T. T. Shun, C. H. Tsau, S. Y. Chang, *Adv. Eng. Mater.* **2004**, *6*, 299–303.
[94] R. Zhang, C. Wang, P. Zou, R. Lin, L. Ma, L. Yin, T. Li, W. Xu, H. Jia, Q. Li, S. Sainio, K. Kisslinger, S. E. Trask, S. N. Ehrlich, Y. Yang, A. M. Kiss, M. Ge, B. J. Polzin, S. J. Lee, W. Xu, Y. Ren, H. L. Xin, *Nature* **2022**, *610*, 67.
[95] N. Yabuuchi, Y.-T. Kim, H. H. Li, Y. Shao-Horn, *Chem. Mater.* **2008**, *20*, 4936–4951.
[96] X. Zeng, C. Zhan, J. Lu, K. Amine, *Chem* **2018**, *4*, 690–704.
[97] B. Jiang, J. Li, B. Luo, Q. Yan, H. Li, L. Liu, L. Chu, Y. Li, Q. Zhang, M. Li, *J. Energy Chem.* **2021**, *60*, 564–571.
[98] S. E. Renfrew, B. D. McCloskey, *J. Am. Chem. Soc.* **2017**, *139*, 17853–17860.
[99] Y. Wu, H. Ming, M. Li, J. Zhang, W. Wahyudi, L. Xie, X. He, J. Wang, Y. Wu, J. Ming, *ACS Energy Lett.* **2019**, *4*, 656–665.
[100] Z. Chen, G.-T. Kim, Y. Guang, D. Bresser, T. Diemant, Y. Huang, M. Copley, R. J. Behm, S. Passerini, Z. Shen, *J. Power Sources* **2018**, *402*, 263–271.
[101] E. Hu, X. Yu, R. Lin, X. Bi, J. Lu, S. Bak, K.-W. Nam, H. L. Xin, C. Jaye, D. A. Fischer, K. Amine, X.-Q. Yang, *Nat. Energy* **2018**, *3*, 690–698.
[102] G.-L. Xu, Q. Liu, K. K. S. Lau, Y. Liu, X. Liu, H. Gao, X. Zhou, M. Zhuang, Y. Ren, J. Li, M. Shao, M. Ouyang, F. Pan, Z. Chen, K. Amine, G. Chen, *Nat. Energy* **2019**, *4*, 484–494.
[103] X. D. Zhang, J. L. Shi, J. Y. Liang, Y. X. Yin, J. N. Zhang, X. Q. Yu, Y. G. Guo, *Adv. Mater.* **2018**, *30*, 1801751.
[104] H. Lin, J. Zheng, Y. Yang, *Mater. Chem. Phys.* **2010**, *119*, 519–523.
[105] C. Wu, H. Li, S. Cao, Z. Li, P. Zeng, J. Chen, X. Zhu, X. Guo, G. Chen, B. Chang, Y. Shen, X. Wang, *J. Colloid Interface Sci.* **2022**, *628*, 1031–1040.
[106] M. Gong, Y. Fu, W. Yao, X. Rao, Q. Zhang, S. Zhong, Q. Sun, H. Cheng, *ACS Appl. Energy Mater.* **2023**, *6*, 1248–1258.
[107] Z. Luo, G. Hu, W. Wang, K. Du, Z. Peng, J. Zeng, L. Li, Y. Cao, *J. Power Sources* **2022**, *548*, 232092.
[108] Z. Chang, Y. Zhang, W. He, J. Wang, H. Zheng, B. Qu, X. Wang, Q. Xie, D.-L. Peng, *Ind. Eng. Chem. Res.* **2022**, *61*, 7464–7473.
[109] J. Cheng, L. Mu, C. Wang, Z. Yang, H. L. Xin, F. Lin, K. A. Persson, *J. Mater. Chem. A* **2020**, *8*, 23293–23303.
[110] W. Yan, S. Yang, Y. Huang, Y. Yang, G. Yuan, *J. Alloys Compd.* **2020**, *819*, 153048.

Manuscript received: June 30, 2024
Revised manuscript received: September 3, 2024
Accepted manuscript online: September 4, 2024
Version of record online: October 31, 2024